QUANTUM OPTICS

Quantum walks and wavepacket dynamics on a lattice with twisted photons

Filippo Cardano,[1] Francesco Massa,[1]* Hammam Qassim,[2] Ebrahim Karimi,[2]
Sergei Slussarenko,[1†] Domenico Paparo,[3] Corrado de Lisio,[1,3] Fabio Sciarrino,[4]
Enrico Santamato,[1] Robert W. Boyd,[2] Lorenzo Marrucci[1,3‡]

The "quantum walk" has emerged recently as a paradigmatic process for the dynamic simulation of complex quantum systems, entanglement production and quantum computation. Hitherto, photonic implementations of quantum walks have mainly been based on multipath interferometric schemes in real space. We report the experimental realization of a discrete quantum walk taking place in the orbital angular momentum space of light, both for a single photon and for two simultaneous photons. In contrast to previous implementations, the whole process develops in a single light beam, with no need of interferometers; it requires optical resources scaling linearly with the number of steps; and it allows flexible control of input and output superposition states. Exploiting the latter property, we explored the system band structure in momentum space and the associated spin-orbit topological features by simulating the quantum dynamics of Gaussian wavepackets. Our demonstration introduces a novel versatile photonic platform for quantum simulations.

INTRODUCTION

First proposed by Feynman about 30 years ago (1), the simulation of a complex quantum system by means of another simpler and well-controlled quantum system is nowadays becoming a feasible, although still challenging, task. Photons are a reliable resource in this arena, as witnessed by the large variety of photonic architectures that have been introduced hitherto for the realization of quantum simulators (2). Among simulated processes, the quantum walk (QW) (3) is receiving wide interest. A QW can be interpreted as the quantum counterpart of the well-known classical random walk. In its simplest, discrete, and one-dimensional (1D) example, the latter is a path consisting of a sequence of random steps along a line. At each step, the walker moves forward or backward according to the outcome of a random process, such as the flip of a coin. When both the walker and the coin are quantum systems, we obtain a QW. The final probability distribution for the walker position shows marked differences with respect to the classical process, due to interferences between coherent superpositions of different paths (4). It has been demonstrated that this quantum process can be used to perform quantum search algorithms on a graph (5, 6) and universal quantum computation (7, 8). Moreover, it represents a versatile approach to the simulation of phenomena characterizing complex systems, such as Anderson localization in disordered media (9) and energy transport in chemical processes (10). The coin-walker interaction, for example, gives rise to fascinating analogies with quantum effects arising from spin-orbit coupling: recently, it was demonstrated that discrete QWs can simulate all classes of topological phases in 1D and 2D (11), and topologically protected bound states have been observed at the interface between regions with different topologies (12).

In the last decade, implementations of QWs in 1D have been realized in a variety of physical systems, such as trapped ions (13, 14) or atoms (15), nuclear magnetic resonance systems (16), and photons, using both bulk optics (17–19) and integrated waveguides (20–22). Remarkably, only a few photonic simulations of multiparticle QWs have been reported, using two-photon states (9, 20–22) or classical coherent sources (23). In photonic architectures, different strategies can be adopted, according to the optical degrees of freedom exploited to encode the coin and the walker quantum systems. In 2010, Zhang et al. proposed a novel approach for the realization of a photonic QW, based on the idea of encoding the coin and the walker in the spin angular momentum (SAM) and in the orbital angular momentum (OAM) of light, respectively (24). A possible implementation of the same idea in a loop-based configuration has been also analyzed (25). These theoretical proposals put forward, for the first time, the possibility of implementing a photonic walk without interferometers, with the whole process taking place within a single light beam (we refer here to "real-space interferometers," relying on optical path splitting, as any kind of wave propagation involves some form of modal interference). To obtain this result, these schemes rely on the spin-orbit coupling occurring in a special optical element called q-plate (QP) (26), whose action will be discussed later on. Here, we implement experimentally the proposal by Zhang et al., thus demonstrating the first photonic QW occurring in a single light beam and using the OAM degree of freedom of photons as discrete walker coordinate [we notice that, although the QW realized in (19) and (23) involves only inner degrees of freedom of a single light beam, its actual implementation still relies on splitting the beam in a spatial interferometer]. We demonstrate both the QW of single photons and that of two indistinguishable photons, thus highlighting the role of multiparticle quantum interferences. As we will discuss further below, this novel implementation has potential advantages in terms of stability and scalability. Moreover, in contrast to most current integrated-optics approaches, it allows one to dynamically vary the Hamiltonian system and to measure the whole evolution step by step (not only the final output) without changing the experimental setup. Finally, a very important feature of this QW implementation is the possibility of flexibly preparing arbitrary superpositions or "delocalized" initial states of the walker by exploiting standard

[1]Dipartimento di Fisica, Università di Napoli Federico II, Complesso Universitario di Monte Sant'Angelo, Napoli 80126, Italy. [2]Department of Physics, University of Ottawa, 150 Louis Pasteur, Ottawa, Ontario K1N 6N5, Canada. [3]CNR-SPIN, Complesso Universitario di Monte Sant'Angelo, Napoli 80126, Italy. [4]Dipartimento di Fisica, Sapienza Università di Roma, Roma 00185, Italy.
*Present address: Faculty of Physics, University of Vienna, Boltzmanngasse 5, 1090 Vienna, Austria.
†Present address: Centre for Quantum Dynamics, Griffith University, Brisbane, Queensland 4111, Australia.
‡Corresponding author. E-mail: marrucci@na.infn.it; lorenzo.marrucci@unina.it

holographic optical devices (or, conversely, to make a full quantum tomography of the delocalized output quantum state). As a specific demonstration of this feature, we experimentally verified the band structure characterizing a QW; we prepared Gaussian wavepackets of a photon in OAM space, for different values of the average linear quasi-momentum, and observed their free quantum dynamics, governed by the underlying band dispersion relations and the associated topological spin-orbit features ([11], [27], [28]).

RESULTS

QW in the OAM space of a photon

In the quantum theory framework, a discrete QW typically involves a system described by a Hilbert space $\mathcal{H}$ obtained by the direct product $\mathcal{H}_c \otimes \mathcal{H}_w$ of the coin and the walker subspaces, respectively. In the simplest case, the walker is moving in a 1D lattice and, at each step, has only two choices. Accordingly, the subspace $\mathcal{H}_c$ is 2D, whereas $\mathcal{H}_w$ is infinite-dimensional; they are spanned by the vectors $\{|\uparrow\rangle_c, |\downarrow\rangle_c\}$ and $\{|x\rangle_w, x \in \mathbb{Z}\}$, respectively (in the following, subscripts c and w will be omitted for brevity whenever there is no risk of ambiguity). Alternatively, the walker state can be described in terms of its quasi-momentum k, which is defined in the first Brillouin zone $k \in (-\pi, \pi)$. The relation between the two representations is given by the discrete Fourier transform, that is, $|k\rangle = (1/\sqrt{2\pi})\sum_x e^{-ikx}|x\rangle$. The momentum representation provides the framework to analyze the effective band structure of the QW system, as will be discussed later on. The displacement of the walker at each step of the process is realized by the shift operator $\hat{S}$

$$\hat{S} = |\uparrow\rangle\langle\uparrow|\otimes\hat{L}^+ + |\downarrow\rangle\langle\downarrow|\otimes\hat{L}^-, \tag{1}$$

where the operators $\hat{L}^\pm$ shift the position of the walker, that is, $\hat{L}^\pm|x\rangle = |x \pm 1\rangle$. The displacement introduced by $\hat{S}$ is conditioned by the coin; when this is in the state $|\uparrow\rangle$, the walker moves up, and vice versa. As a consequence, the operator $\hat{S}$ entangles the coin and the walker systems ([27], [29]). Between consecutive displacements, the "randomness" is introduced by a unitary operator $\hat{T}$ acting on the coin subspace, as generally given by $\hat{T}|\uparrow\rangle = a|\uparrow\rangle + b|\downarrow\rangle$ and $\hat{T}|\downarrow\rangle = b^*|\uparrow\rangle - a^*|\downarrow\rangle$ (up to a global phase), with a,b complex numbers such that $|a|^2 + |b|^2 = 1$; for an unbiased walk, $|a| = |b| = 1/\sqrt{2}$. A single step of the walk is described by the step operator $\hat{U} = \hat{S} \cdot (\hat{T} \otimes \hat{I}_w)$, where $\hat{I}_w$ is the identity operator in $\mathcal{H}_w$. After n steps, the system initially prepared in the state $|\psi_0\rangle$ evolves to a new state

$$|\psi_n\rangle = \hat{U}^n|\psi_0\rangle \tag{2}$$

In the momentum representation, eigenstates of the operator $\hat{U}$ have a simple expression ([11], [27]), given by $|k, s\rangle = |\phi_s(k)\rangle_c \otimes |k\rangle_w$ with eigenvalues $e^{-i\omega_s(k)}$, where $s \in \{1, 2\}$. The dispersion relation of quasi-energies $w_s(k)$ shows two gapped bands associated with the coin eigenstates $|\phi_s(k)\rangle$, whereas the parametric dependence of the latter states on k defines the QW topological structure ([28]). A more detailed analysis of these QW properties is provided in the Supplementary Materials.

Consider now a photon and its internal degrees of freedom represented by the SAM and the OAM. In the limit of paraxial optics, these two quantities are independent and well defined; the first is associated with the polarization of the light, whereas the second is related to the azimuthal structure of the optical wavefront in the transverse plane ([30]). The SAM space is spanned by vectors $\{|L\rangle, |R\rangle\}$, representing left circular and right

circular polarizations. The OAM space is spanned by vectors $|m\rangle$ with $m \in \mathbb{Z}$, which denote a photon carrying $m\hbar$ of OAM along the propagation axis, where $\hbar$ is the reduced Planck constant, and having a correspondingly "twisted" wave function (see Fig. 1).

In our implementation, the coin and the walker systems are encoded in the SAM and the OAM of a photon, respectively. In particular, the spatial walker coordinate x is replaced by the OAM coordinate m. The concept of a QW in OAM within a single optical beam is pictorially illustrated in Fig. 1. The step operator $\hat{U}$ is realized by means of linear optical elements. In the coin subspace, the unitary operator $\hat{T}$ can be implemented by birefringent plates, such as quarter-wave plates (QWP) and/or half-wave plates (HWP). In particular, we used only wave plate combinations giving rise to unbiased QWs. The shift operator $\hat{S}$ is realized by a QP, a recently introduced photonic device that has already found many useful applications in classical and quantum optics ([26], [30–33]). The QP is a birefringent liquid-crystal medium with an inhomogeneous optical axis that has been arranged in a singular pattern, with topological charge q, so as to give rise to an engineered spin-orbit coupling in the light crossing it. In particular, the QP raises or lowers the OAM of the incoming photon according to its SAM state, while leaving the photon in the same optical beam, that is, with no deflections or diffractions. In the actual device, the radial profile of the photonic wave function undergoes a small alteration, which however can be approximately neglected in our implementation, as discussed in the Supplementary Materials. More precisely, the action of a QP can be generally described by the operator $\hat{Q}_\delta$

$$\hat{Q}_\delta|L, m\rangle = \cos(\delta/2)|L, m\rangle - i \sin(\delta/2)|R, m + 2q\rangle$$

$$\hat{Q}_\delta|R, m\rangle = \cos(\delta/2)|R, m\rangle - i \sin(\delta/2)|L, m - 2q\rangle, \tag{3}$$

where q is the topological charge of the QP, and δ is the optical birefringent phase-retardation ([26], [30]). Whereas q is a fixed property of the QP, δ can be controlled dynamically by tuning an applied voltage ([34]). As shown in Eq. 3, the action of the QP is made of two terms. The first, proportional to $\cos(\delta/2)$, leaves the photon in its input state. The second, proportional to $\sin(\delta/2)$, implements the conditional displacement of Eq. 1, but also adds a flip of the coin state. The latter effect can be compensated by inserting an additional HWP. When $\delta = \pi$
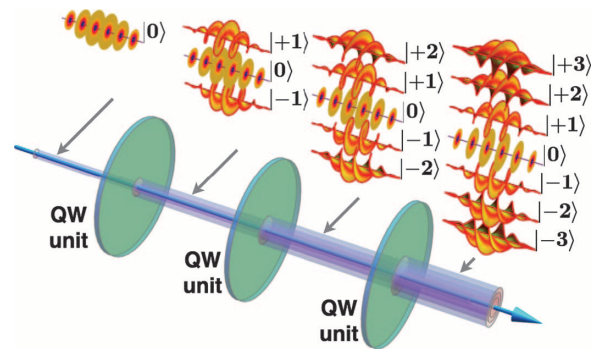
Fig. 1. Conceptual scheme of the single-beam photonic QW in the space of OAM. In each traversed optical stage (QW unit), the photon can move to an OAM value m that can increase or decrease by one unit (or stay still, in the hybrid configuration). The OAM decomposition of the photonic wave function at each stage thus includes many different components, as shown in the callouts in which modes having different OAM values are represented by the corresponding helical (or "twisted") wavefronts.

("standard" configuration), the first term vanishes and the standard shift operator $\hat{S}$ is obtained. When $\delta = 0$, the evolution is trivial (the walker stands still), whereas for intermediate values $0 < \delta < \pi$, we have a novel kind of evolution: besides moving forward or backward, the walker at each step is provided with a third option, that is, to remain in the same position. We refer to this as a "hybrid" configuration because it mimics a walk with three possible choices, although the coin is still 2D. Similar to an effective mass, the δ parameter controls the degree of mobility of the walker, ranging from a vanishing mobility for $\delta = 0$ to a maximal mobility (not taking into account the effect of the coin) for $\delta = \pi$.

Single-photon QW with localized initial state

In our first experiment, the step operator $\hat{U}$ is implemented by a sequence of a QWP, a QP, and a HWP. The QPs have $q = 1/2$, so as to induce OAM shifts of ± 1. Because of reflection losses (mainly at the QP, which is not antireflection-coated), each step has a transmission efficiency of 86% (but adding an antireflection coating could easily improve this value to >95%). The n-step walk is then implemented by simply cascading a sequence of QWP-QP-HWP on the single optical axis of the system. In the implemented setup, the linear distance d between adjacent steps is small compared to the Rayleigh range z_R of the photons, that is, $d/z_R \ll 1$ (near-field regime), so as to avoid optical effects that would alter the nature of the simulated process; a detailed discussion is provided in the Supplementary Materials. The layout of the apparatus is shown in Fig. 2. A photon pair is generated by spontaneous parametric down-conversion (SPDC) in the product state $|H\rangle|V\rangle$, where H and V stand for horizontal and vertical linear polarization (see the caption of Fig. 2 for details). To carry out a single-particle QW simulation, we split the two input photons with a polarizing beam splitter (PBS); the H-polarized photon only enters the QW setup after being coupled into a single-mode optical fiber (SMF), which sets $m = 0$. At the exit of the fiber, the initial polarization of the photon is recovered using a QWP-HWP set (not shown in the figure). The V-polarized photon, reflected at the PBS, is sent directly to a detector and provides a trigger, so as to operate the QW simulation in a heralded single-photon quantum regime.

The photon entering the QW setup is initially prepared in a separable state $|\psi_0\rangle = |\phi_0\rangle_c \otimes |\psi_0\rangle_w$. A computer-generated hologram displayed on a spatial light modulator (SLM 1) is used to prepare the walker initial state in a generic superposition of OAM states (35, 36) in $\mathcal{H}_w$ (see the Supplementary Materials for details). After the SLM 1, the coin is prepared in the state $|\phi_0\rangle_c = \alpha|L\rangle + \beta|R\rangle$, where the two complex coefficients α and β (with $|\alpha|^2 + |\beta|^2 = 1$) can be selected at will by a QWP-HWP set (apart from an unimportant global phase). The photon then undergoes the QW evolution and, at the exit, is analyzed in both polarization and OAM so as to determine the output probabilities. Details on projective measurements in OAM are given in the Supplementary Materials.

In the already mentioned first set of experiments, we carried out QWs with single photons prepared in the localized state $m = 0$ on the OAM lattice, with varying SAM input states. In Fig. 3, we report the experimental and predicted results relative to a four-step QW, for two possible input polarization states, and both in the standard and hybrid configurations (two additional input polarization cases are given in fig. S3). To evaluate quantitatively the agreement between measured and predicted probability distributions, $P(m)$ and $P'(m)$, we also computed their "similarity" $S = \left(\sum_m \sqrt{P(m)P'(m)} \right)^2 / (\sum_m P(m) \sum_m P'(m))$. The values we obtain in the various cases are given in the figure captions.

Simulation of wavepacket dynamics in OAM space

Next, exploiting the possibility to control the walker initial state, we investigated the QW evolution for states with a given quasi-momentum k, thus probing the dispersion relation of the effective band structure of our QW system and its associated topological structure (for the standard case with $\delta = \pi$). A similar approach was used to simulate the evolution of a multiband Bloch particle in a time-dependent field, by shining an engineered waveguide array with classical coherent light (37) [see also (38) for a review on discrete-waveguide lattice effects]. Controlling the quasi-momentum of delocalized quantum states is crucial for carrying out quantum simulations of Bloch-particle dynamics, as shown for instance in (39).

Using the holographic method described in the Supplementary Materials, we prepared single-photon wavepackets given by $|\psi_0^s\rangle = |\phi_s(k_0)\rangle_c \otimes (\sum_m A(m)e^{-ik_0m}|m\rangle_w)$, where $A(m) = A_0 e^{-m^2/2\sigma^2}$ is a Gaussian
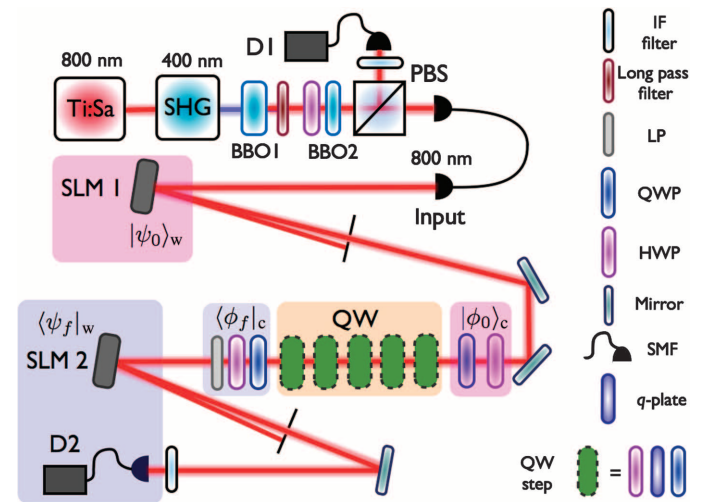
Fig. 2. Experimental apparatus for single-photon QW experiments. Frequency-doubled laser pulses at 400 nm and with 140-mW average power, obtained from the fundamental pulses (100 fs) generated by a titanium:sapphire source (Ti:Sa) at a repetition rate of 82 MHz, pump a 3-mm-thick nonlinear β-barium borate crystal (BBO1) cut for type II SPDC (see main text for a definition of all acronyms). Photon pairs at 800 nm generated through this process, cleaned from residual radiation at 400 nm using a long pass filter, pass through an HWP and the BBO2 crystal (cut as BBO1, but 1.5 mm thick) to compensate both spatial and temporal walk-off introduced by BBO1. Next, the two photons are split by a PBS; one is sent directly to the avalanche single-photon detector (APD) D1, whereas the other is coupled into an SMF. At the exit of the fiber, the photon goes through N identical subsequent QW steps ($N = 5$ in the figure), is then analyzed in both polarization and OAM, and is finally detected with APD D2, in coincidence with D1. Before entering the first QW step, an SLM 1 and an HWP-QWP set are used to prepare the photon initial state in the OAM and SAM spaces, respectively. At the exit of the last step, the polarization projection on the state $|\phi_f\rangle_c$ is performed with a second HWP-QWP set followed by a linear polarizer (LP). The OAM state is then analyzed by diffraction on SLM 2, followed by coupling into a SMF. The projection state $|\psi_f\rangle_w$ corresponding to each OAM eigenvalue m was thus fixed by the hologram pattern displayed on SLM 2. Before detection, interferential filters (IF) centered at 800 nm and with a bandwidth of 3.6 nm were used for spectral cleaning. As shown in the legend, a single QW step consists of a QWP (optical axis at 45° from the horizontal), a QP with $q = 1/2$ (axis at 0°), and an HWP (axis at 0°); the HWP was not included in the wavepacket and two-photon experiments.
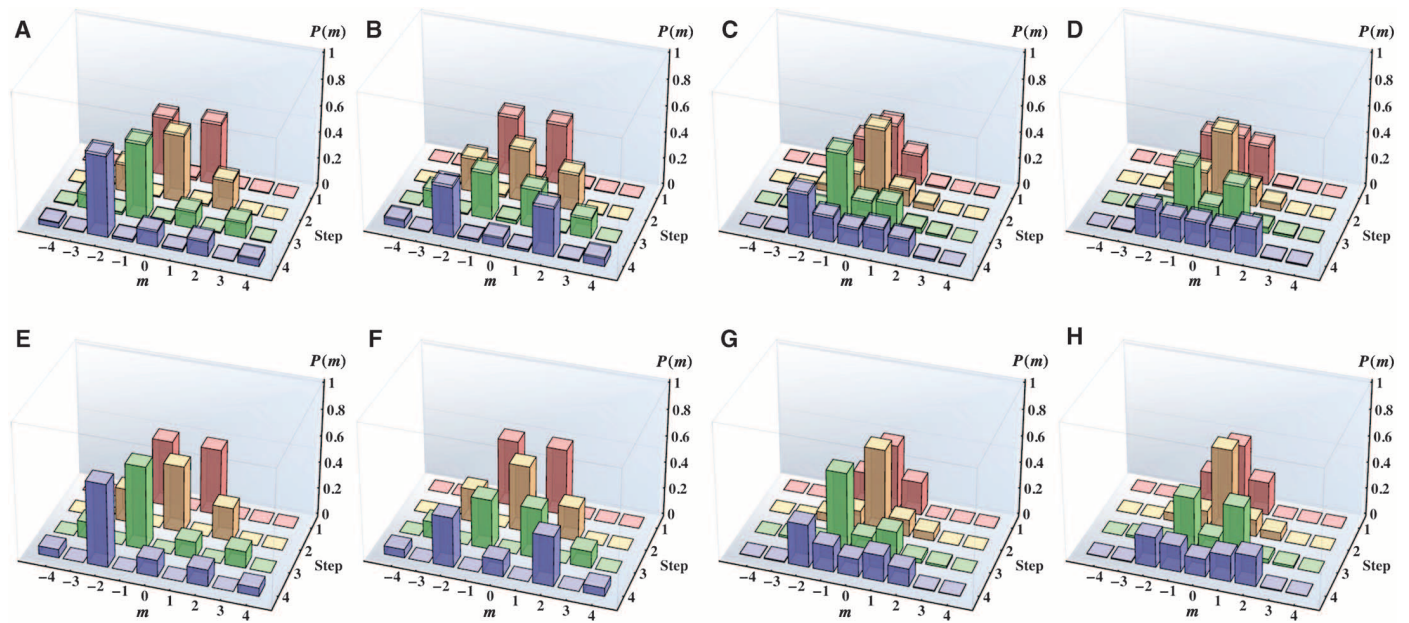
Fig. 3. Four-step QW for a single photon with localized input. (**A** to **D**) Experimental results, including both intermediate and final probabilities for different OAM states in the evolution (summed over different polarizations). The intermediate probabilities at step n are obtained by switching off all QPs that follow that step, that is, setting $\delta = 0$. (A) and (B) refer to the standard case with two different input states for the coin subsystem, $(\alpha, \beta) = (0, 1)$ and $1/\sqrt{2}\,(1, i)$, respectively. (C) and (D) refer to the hybrid case with $\delta =$ 1.57, with the same initial coin-states. (**E** to **H**) Corresponding theoretical predictions. Poissonian statistical uncertainties at ±1 standard deviation are shown as transparent volumes in (A) to (E). The similarities between experimental and predicted final OAM distributions are 94.7 ± 0.4%, 93.4 ± 0.5%, 99.7 ± 0.1%, and 99.2 ± 0.2%, respectively. Panels on the same column refer to the same configuration and initial states. The color scale reflects the number of steps.

envelope in OAM space, and $|\phi_s(k_0)\rangle_c$ (with $s = 1, 2$) is the polarization-coin part of the step-operator eigenstate (11). The associated quasi-momentum has a Gaussian distribution centered on k_0 (incidentally, the average quasi-momentum k_0 corresponds also to the average azimuthal angle in real space for the optical field distribution within the beam). When $A(m)$ is a slowly varying envelope, these wavepackets are expected to propagate on the 1D lattice with only minimal shape variations and with a speed given by the group velocity $V_s(k_0) = (d\omega_s/dk)_{k=k_0}$. States belonging to different bands, which correspond to orthogonal polarization eigenstates, propagate in opposite directions, that is, $V_1(k_0) = -V_2(k_0)$, highlighting the strong spin-orbit coupling of this system (see Supplementary Materials for more details).

In Fig. 4, we report the experimental "real-time" (that is, step-by-step) observation of these propagating packets for a five-step QW. These data refer in particular to the band $s = 1$, with $k_0 = \pi$ and $k_0 = \pi/2$, corresponding to maximum and vanishing group velocities, respectively, with a step operator implemented by a QP plus a QWP. Next, we proceeded to explore the whole irreducible Brillouin zone by varying the average quasi-momentum k_0 in steps of $\pi/8$ across the $(0, \pi)$ range. At each value of k_0, in order to obtain a single wavepacket propagation, the SAM input state must be prepared in the eigenstate $|\phi_1(k_0)\rangle$, corresponding to a specific elliptical polarization. As a result of the so-called sublattice or chiral symmetry (11), the corresponding SAM (or coin) eigenstates of these wavepackets describe a maximum circle in the Poincaré polarization sphere, as illustrated in Fig. 5A. The number of full rotations of the vector $|\phi_1(k)\rangle$ on the sphere, as k varies from $-\pi$ to π, is a topological property of the QW system. In our case, we observe a single full rotation (we actually see half a rotation, as we tested

only half of the Brillouin zone), thus verifying the topological class of our system. Other topological QW phases could be realized by modifying the QW step operator $\hat{U}$, as discussed in (11). We then determined the group velocity of these wavepackets by measuring the mean OAM exit value after five steps, as shown in Fig. 5B. The whole OAM distribution for some of these points is also shown in Fig. 5 (C to G).

Finally, the behavior of a wavepacket whose coin is prepared in the superposition state $(|\phi_1(k_0)\rangle + |\phi_2(k_0)\rangle)/\sqrt{2}$ was also investigated. As a result of the spin-orbit coupling, the wavepacket splits into two components propagating in opposite directions, as shown in Fig. 5H. In this example, the QW clearly leads to the generation of entanglement between the SAM and OAM degrees of freedom. The large average OAM separation obtained between the two wavepacket components implies that the obtained final photon state can be interpreted as a Schrödinger "cat state" in OAM space.

Two-photon QW

The experiments discussed above were carried out in the heralded single-photon regime. Although the latter is a quantum regime, it behaves equivalently to a classical one, as the resulting probability distributions are identical to the intensity distributions that would be obtained using classical (coherent) light. However, the OAM QW platform introduced in this work is also immediately suitable for simulating multiparticle quantum processes, for which quantum interferences cannot be reproduced classically.

To provide a first demonstration of this additional feature, we investigated the simultaneous QW of two identical photons. In this case, both photons generated in the SPDC process were sent to the QW setup, after
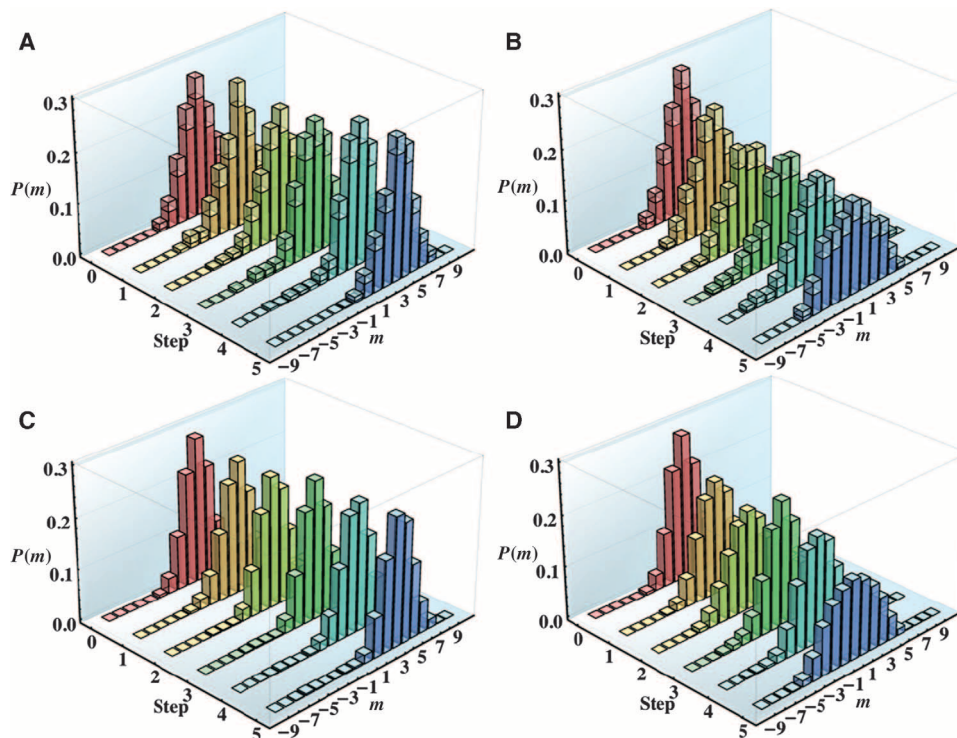
Fig. 4. Wavepacket propagation in a five-step QW. (A and **B)** Experimental results, showing the step-by-step evolution of the OAM distribution of a single photon prepared in a Gaussian wavepacket with $\sigma = 2$, in the SAM band $s = 1$ (summed over different polarizations). (A) and (B) correspond to the two cases $k_0 = \pi$ (maximal group velocity) and $k_0 = \pi/2$ (vanishing group velocity), respectively. The latter configuration shows some spreading of the Gaussian envelope, governed by the group velocity dispersion. Poissonian statistical uncertainties at ±1 SD are shown as transparent volumes. (**C** and **D)** Theoretical predictions corresponding to the same cases. At the fifth step, the similarities between experimental and theoretical OAM distributions are 98.2 ± 0.4% and 99.0 ± 0.2%, respectively. The color scale reflects the number of steps.

adjusting their input polarization state to $|R\rangle|L\rangle$, selected as a typical case. At the exit of the QW cascade, we split the two photons with a beam splitter (BS) and analyzed them in both polarization and OAM, so as to obtain their joint probability distribution (see fig. S4 for the experimental layout). In Fig. 6, the results relative to a three-step QW with localized OAM input $m = 0$ are reported and compared with the theoretical predictions obtained for indistinguishable photons (while taking into account the effect of the final beam splitter), hereafter labeled as "indistinguishable-photon theory" (IPT). The two distributions show a good quantitative agreement, as confirmed by their similarities being higher than 95% (see figure captions for details). These similarities are defined as in the single photon case, with the index m replaced by the pair of OAM values (m_1, m_2). The predicted distributions for the case of distinguishable photons (DPT) are also shown for comparison to highlight the role of two-particle interference in the final distributions. The similarities of the data with the DPT distributions are significantly lower. However, the similarity is not a very sensitive test, because it tends to remain high even for fairly different distributions. Hence, we also computed the "total variation distance" (TVD; defined as the sum of the absolute values of all probability differences divided by two) for the two cases. In the standard case, the TVD of the experimental distribution with the IPT one is 6.5 ± 0.9%, to be compared with the TVD of 16.5 ± 0.9% for the DPT model. In the hybrid case, the TVD

with the IPT is 13.5 ± 0.7%, to be compared with 21.1 ± 0.7% for the DPT. These values confirm that two-photon interferences are present in our experiment. We ascribe the residual discrepancies between the observed distributions and the IPT quantum predictions to systematic errors arising from imperfect alignment of the setup.

On the other hand, it is also possible to demonstrate a quantum behavior in the observed distributions independently of any specific model for the photon propagation in the QW system, so as to be insensitive to alignment imperfections or other kinds of systematic errors. As discussed in the Supplementary Materials, this is accomplished by testing the violation of certain characteristic inequalities that constrain any possible correlation distribution obtained with two classical light sources instead of two photons (20), or with two distinguishable photons. The measured distributions indeed violate these inequalities by several SDs, as illustrated in the Supplementary Materials (figs. S6 and S7). This proves once more that the measured correlations must be quantum and that they include the effect of multiparticle interference.

DISCUSSION

In this article, we have demonstrated a single- and multiphoton QW simulator based on single beam propagation through linear optical devices. The realized architecture is efficient and stable. Moreover, in contrast to other photonic QW implementations, the number of optical components employed scales only linearly with the number of steps, because at each step all OAM values are addressed simultaneously by a single optical element, whose transverse extension remains constant. It must be noted, however, that this advantage in scaling remains valid only as long as the entire QW takes place in the optical near-field, where the beam cross-section size will remain approximately constant, whereas in the far-field, the transverse size of the optical components will have to increase with the OAM range (see the Supplementary Materials).

An important advantage of this platform is the possibility to prepare the walker initial state, even if extended over many lattice sites, with high accuracy and flexibility. We exploited this feature to investigate the effective band structure of QWs, demonstrating the propagation of Gaussian wavepackets for different points in the Brillouin zone and exploring the
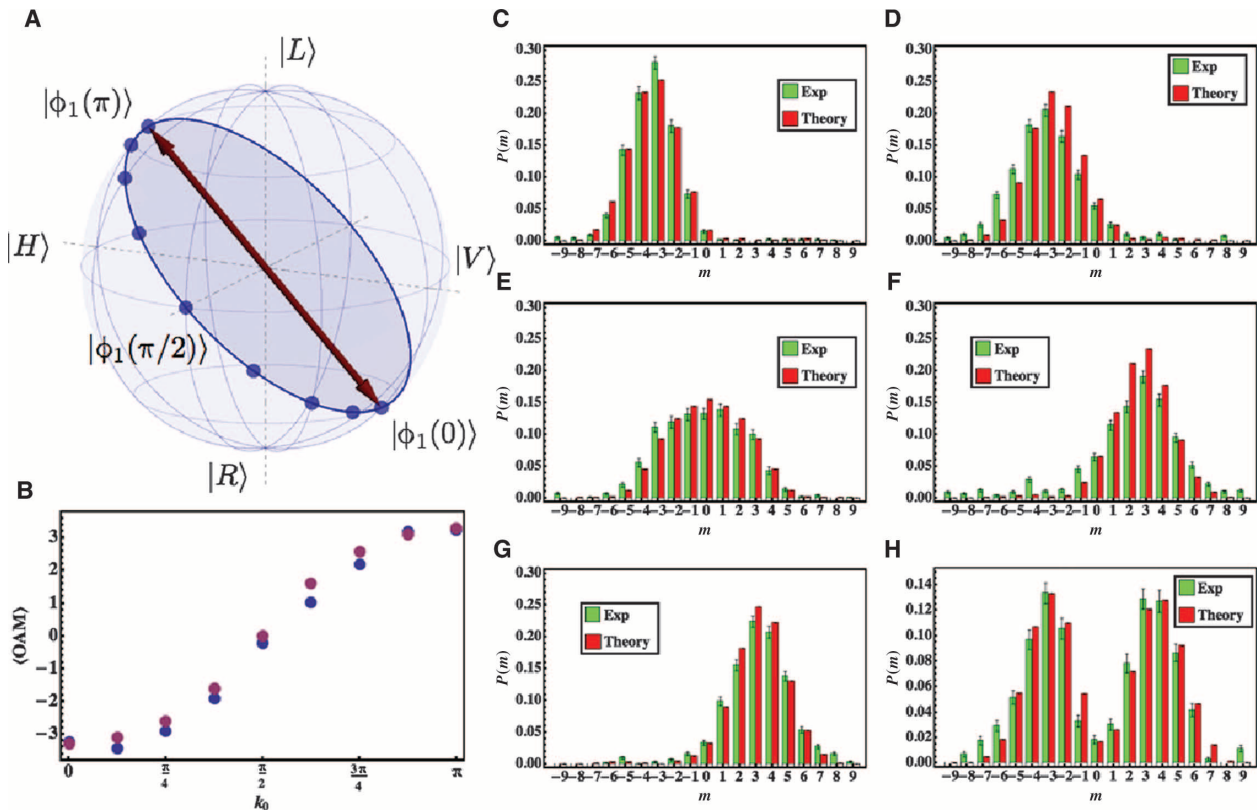
Fig. 5. QW wavepacket dispersion properties in the Brillouin zone. (**A**) Poincaré sphere representation of the polarization (or SAM) eigen-states $|\phi_1(k)\rangle$ prepared in our experiments, for different values of the quasi-momentum k in the irreducible Brillouin zone $(0, \pi)$ taken in steps of $\pi/8$ (blue dots). These states lie on a maximal circle (blue line) of the sphere. (**B**) Mean OAM after a five-step QW for a single photon prepared in a Gaussian wave-packet with $\sigma = 2$ and $s = 1$, with different values of average quasi-momentum k_0 in the range $(0, \pi)$. Blue and purple points are associated to experimental data and theoretical predictions, respectively; Poissonian statistical uncertainties are too small to be shown in the graph. (**C** to **G**) Final OAM distribution associated to some of these cases (summed over different polarizations). Panels refer to $k_0 = 0, \pi/4, \pi/2, 3\pi/4, \pi$, respectively. (**H**) OAM distribution after a five-step QW for a wavepacket whose coin is prepared in the superposition state $(|\phi_1(0)\rangle + |\phi_2(0)\rangle)/\sqrt{2}$. As predicted by the theory, it splits into two components propagating in opposite directions, thus generating a maximally entangled SAM-OAM state. In (C) to (H), Poissonian statistical uncertainties at ± 1 SD are shown by error bars. The similarities between experimental and theoretical OAM distributions are $98.9 \pm 0.2\%$, $96.2 \pm 0.4\%$, $98.4 \pm 0.3\%$, $93.2 \pm 0.6\%$, $99.1 \pm 0.2\%$, and $97.3 \pm 0.4\%$, respectively.

associated topological structure arising from the spin-orbit coupling. For a certain initial state, the wavepacket is split in two by the QW evolution, leading to a quantum "Schrödinger cat state" in OAM. In prospect, it will be very interesting to simulate the quantum propagation of extended states of two (or more) photons, possibly entangled to each other, such as those naturally generated in the SPDC process. Moreover, engineering the initial state of the walker is a possible strategy for the simulation of complex QW dynamics through the combination of suitable delocalized initial conditions plus a standard QW evolution; a theoretical proposal was reported recently for the case of "driven QWs" (40).

A current limitation of our approach is that the walk evolution cannot be position-dependent (that is, OAM-dependent), in contrast to other implementations (9, 23). This limitation could be overcome in the future by introducing additional optical elements acting on the azimuthal coordinate (for example, a Dove's prism can introduce an OAM-dependent phase shift) or by exploiting the radial beam coordinate, which couples with OAM in free propagation and can be acted on by a radially patterned optical element. On the other hand, our approach allows very convenient and easy control of the evolution operator at each step, including the possibility of fully automated fast switching of its properties by introducing electro-optical devices to manipulate the polarization or by electrically controlling the QP tuning. This may enable, for example, the simulation of a quantum system having a time-dependent Hamiltonian or that of a statistical ensemble of quantum systems with different Hamiltonians. Another potential advantage of the present implementation is the possibility to carry out a full quantum tomography of the outgoing state, which is very challenging for standard interferometric implementations. Finally, we must mention the important limitation of our platform, common to all fully photonic QW implementations, of not being able to simulate particle interactions. A possible future strategy to overcome this limitation might be based on ideas similar to those proposed by Knill *et al.* for doing quantum computation with linear optics (41, 42).
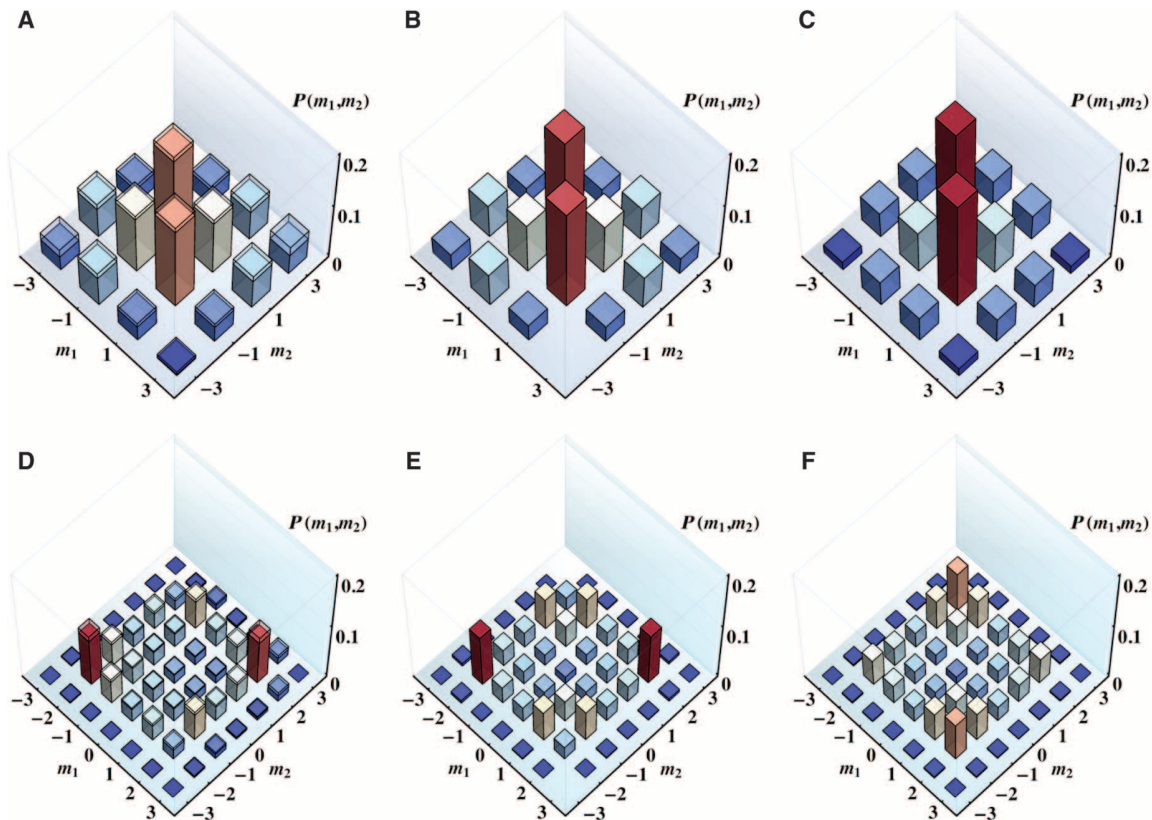
SUPPLEMENTARY MATERIALS

Fig. 6. Three-step QW for two identical photons. In this case, only final OAM probabilities are shown (summed over different polarizations). (**A** to **C**) Case of standard walk. (A) Experimental results. Vertical bars represent estimated joint probabilities for the OAM of the two photons. Because the two measured photons detected after the BS splitting are physically equivalent, their counts are averaged together, so that (m_1, m_2) and (m_2, m_1) pairs actually refer to the same piece of data. Even values of m_1 and m_2 are not included because they correspond to sites that cannot be occupied after an odd number of steps. (B) Theoretical predictions for the case of indistinguishable photons. (C) Theoretical predictions for the case of distinguishable photons, shown to highlight the effect of two-photon interference (Hong-Ou-Mandel effect) in the final probabilities. It can be seen that the experimental results

agree better with the theory for indistinguishable photons. (**D** to **F**) Case of hybrid walk (with $\delta = 1.46$). (D), (E), and (F) refer, respectively, to experimental data, indistinguishable photon theory, and distinguishable photon theory, as in the previous case. The QW step in these two-photon experiments is implemented with a QP and a QWP. Again, our experiment is in good agreement with the theory based on indistinguishable photons, proving that two-photon interferences are successfully implemented in our experiment. The similarities between experimental and predicted quantum distributions (IPT model) are $98.2 \pm 0.4\%$ and $95.8 \pm 0.3\%$ for the standard and the hybrid walk, respectively. The similarities with the DPT model are, instead, 96.4 and 91.8%, respectively. The color scale (common to all panels referring to the same case) reflects the vertical scale, to help compare the patterns.

Fig. S4. Two-photon QW apparatus.

Fig. S5. Experimental verification of the indistinguishability of the two-photon source through polarization Hong-Ou-Mandel (HOM) interference.

Fig. S6. Experimental violation of correlation inequalities for two photons that have completed the standard QW ($\delta = \pi$).

Fig. S7. Experimental violation of correlation inequalities for two photons that have completed the hybrid QW ($\delta = \pi/2$).

Table S1. Power coefficients of the various p-index terms appearing in the expansion of the beam emerging from a QP (with $q = 1/2$) in the LG mode basis, assuming that the input is an L-polarized LG mode with $p = 0$ and the given OAM m value.

REFERENCES AND NOTES

1. R. Feynman, Simulating physics with computers. *Int. J. Theor. Phys.* **21**, 467–488 (1982).
2. A. Aspuru-Guzik, P. Walther, Photonic quantum simulators. *Nat. Phys.* **8**, 285–291 (2012).
3. J. Kempe, Quantum random walks: An introductory overview. *Contemp. Phys.* **44**, 307–327 (2003).
4. P. L. Knight, E. Roldán, J. E. Sipe, Quantum walk on the line as an interference phenomenon. *Phys. Rev. A* **68**, 020301 (2003).
5. N. Shenvi, J. Kempe, B. Whaley, Quantum random walk search algorithm. *Phys. Rev. A* **67**, 052307 (2003).
6. V. Potoček, A. Gábris, T. Kiss, I. Jex, Optimized quantum random-walk search algorithms on the hypercube. *Phys. Rev. A* **79**, 012325 (2009).
7. A. M. Childs, Universal computation by quantum walk. *Phys. Rev. Lett.* **102**, 180501 (2009).
8. N. B. Lovett, S. Cooper, M. Everitt, M. Trevers, V. Kendon, Universal quantum computation using the discrete-time quantum walk. *Phys. Rev. A* **81**, 042330 (2010).
9. A. Crespi, R. Osellame, R. Ramponi, V. Giovannetti, R. Fazio, L. Sansoni, F. De Nicola, F. Sciarrino, P. Mataloni, Anderson localization of entangled photons in an integrated quantum walk. *Nature Photon.* **7**, 322–328 (2013).
10. M. Mohseni, P. Rebentrost, S. Lloyd, A. Aspuru-Guzik, Environment-assisted quantum walks in photosynthetic energy transfer. *J. Chem. Phys.* **129**, 174106 (2008).
11. T. M. S. Rudner Kitagawa, E. Berg, E. Demler, Exploring topological phases with quantum walks. *Phys. Rev. A* **82**, 033429 (2010).
12. T. Kitagawa, M. A. Broome, A. Fedrizzi, M. S. Rudner, E. Berg, I. Kassal, A. Aspuru-Guzik, E. Demler, A. G. White, Observation of topologically protected bound states in photonic quantum walks. *Nat. Commun.* **3**, 882 (2012).
13. H. Schmitz, R. Matjeschk, C. Schneider, J. Glueckert, M. Enderlein, T. Huber, T. Schaetz, Quantum walk of a trapped ion in phase space. *Phys. Rev. Lett.* **103**, 090504 (2009).
14. F. Zähringer, G. Kirchmair, R. Gerritsma, E. Solano, R. Blatt, C. F. Roos, Realization of a quantum walk with one and two trapped ions. *Phys. Rev. Lett.* **104**, 100503 (2010).
15. M. Karski, L. Förster, J. M. Choi, A. Steffen, W. Alt, D. Meschede, A. Widera, Quantum walk in position space with single optically trapped atoms. *Science* **325**, 174–177 (2009).

Cardano *et al. Sci. Adv.* 2015;1:e1500087   13 March 2015

7 of 8

16. C. A. Ryan, M. Laforest, J. C. Boileau, R. Laflamme, Experimental implementation of a discrete-time quantum random walk on an NMR quantum-information processor. *Phys. Rev. A* **72**, 062317 (2005).

17. P. Zhang, X. F. Ren, X. B. Zou, B. H. Liu, Y. F. Huang, G. C. Guo, Demonstration of one-dimensional quantum random walks using orbital angular momentum of photons. *Phys. Rev. A* **75**, 052310 (2007).

18. M. A. Broome, A. Fedrizzi, B. P. Lanyon, I. Kassal, A. Aspuru-Guzik, A. G. White, Discrete single-photon quantum walks with tunable decoherence. *Phys. Rev. Lett.* **104**, 153602 (2010).

19. A. Schreiber, K. N. Cassemiro, V. Potocek, A. Gábris, P. J. Mosley, E. Andersson, I. Jex, Ch. Silberhorn, Photons walking the line: A quantum walk with adjustable coin operations. *Phys. Rev. Lett.* **104**, 050502 (2010).

20. A. Peruzzo, M. Lobino, J. C. F. Matthews, N. Matsuda, A. Politi, K. Poulios, X. Zhou, Y. Lahini, N. Ismail, K. Worhoff, Y. Bromberg, Y. Silberberg, M. G. Thompson, J. L. O'Brien, Quantum walks of correlated photons. *Science* **329**, 1500–1503 (2010).

21. J. O. Owens, M. A. Broome, D. N. Biggerstaff, M. E. Goggin, A. Fedrizzi, T. Linjordet, M. Ams, G. D. Marshall, J. Twamley, M. J. Withford, A. G. White, Two-photon quantum walks in an elliptical direct-write waveguide array. *New J. Phys.* **13**, 075003 (2011).

22. L. Sansoni, F. Sciarrino, G. Vallone, P. Mataloni, A. Crespi, R. Ramponi, R. Osellame, Two-particle bosonic-fermionic quantum walk via integrated photonics. *Phys. Rev. Lett.* **108**, 010502 (2012).

23. A. Schreiber, A. Gábris, P. P. Rohde, K. Laiho, M. Štefaňák, V. Potoček, C. Hamilton, I. Jex, C. Silberhorn, A 2D quantum walk simulation of two-particle dynamics. *Science* **336**, 55–58 (2012).

24. P. Zhang, B. H. Liu, R. F. Liu, H. R. Li, F. L. Li, G. C. Guo, Implementation of one-dimensional quantum walks on spin-orbital angular momentum space of photons. *Phys. Rev. A* **81**, 052322 (2010).

25. S. K. Goyal, F. S. Roux, A. Forbes, T. Konrad, Implementing quantum walks using orbital angular momentum of classical light. *Phys. Rev. Lett.* **110**, 263602 (2013).

26. L. Marrucci, C. Manzo, D. Paparo, Optical spin-to-orbital angular momentum conversion in inhomogeneous anisotropic media. *Phys. Rev. Lett.* **96**, 163905 (2006).

27. G. Abal, R. Siri, A. Romanelli, R. Donangelo, Quantum walk on the line: Entanglement and nonlocal initial conditions. *Phys. Rev. A* **73**, 042302 (2006).

28. T. Kitagawa, Topological phenomena in quantum walks: Elementary introduction to the physics of topological phases. *Quantum Inf. Process.* **11**, 1107–1148 (2012).

29. R. Vieira, E. P. M. Amorim, G. Rigolin, Dynamically disordered quantum walk as a maximal entanglement generator. *Phys. Rev. Lett.* **111**, 180503 (2013).

30. L. Marrucci, E. Karimi, S. Slussarenko, B. Piccirillo, E. Santamato, E. Nagali, F. Sciarrino, Spin-to-orbital conversion of the angular momentum of light and its classical and quantum applications. *J. Opt.* **13**, 064001 (2011).

31. F. Cardano, E. Karimi, S. Slussarenko, L. Marrucci, C. de Lisio, E. Santamato, Polarization pattern of vector vortex beams generated by q-plates with different topological charges. *Appl. Opt.* **51**, C1–C6 (2012).

32. D'Ambrosio, V., E. Nagali, S. P. Walborn, L. Aolita, S. Slussarenko, L. Marrucci, F. Sciarrino, Complete experimental toolbox for alignment-free quantum communication. *Nat. Commun.* **3**, 961 (2012).

33. V. D'Ambrosio, N. Spagnolo, L. Del Re, S. Slussarenko, Y. Li, L. C. Kwek, L. Marrucci, S. P. Walborn, L. Aolita, F. Sciarrino, Photonic polarization gears for ultra-sensitive angular measurements. *Nat. Commun.* **4**, 2432 (2013).

34. B. Piccirillo, V. D'Ambrosio, S. Slussarenko, L. Marrucci, E. Santamato, Photon spin-to-orbital angular momentum conversion via an electrically tunable q-plate. *Appl. Phys. Lett.* **97**, 241104 (2010).

35. E. Bolduc, N. Bent, E. Santamato, E. Karimi, R. W. Boyd, Exact solution to simultaneous intensity and phase encryption with a single phase-only hologram. *Opt. Lett.* **38**, 3546–3549 (2013).

36. V. D'Ambrosio, F. Cardano, E. Karimi, E. Nagali, E. Santamato, L. Marrucci, F. Sciarrino, Test of mutually unbiased bases for six-dimensional photonic quantum systems. *Sci. Rep.* **3**, 2726 (2013).

37. S. Longhi, M. Lobino, M. Marangoni, R. Ramponi, P. Laporta, E. Cianci, V. Foglietti, Semi-classical motion of a multiband Bloch particle in a time-dependent field: Optical visualization. *Phys. Rev. B* **74**, 155116 (2006).

38. D. N. Christodoulides, F. Lederer, Y. Silberberg, Discretizing light behaviour in linear and nonlinear waveguide lattices. *Nature* **424**, 817–823 (2003).

39. M. Atala, M. Aidelsburger, J. T. Barreiro, D. Abanin, T. Kitagawa, E. Demler, I. Bloch, Direct measurement of the Zak phase in topological Bloch bands. *Nat. Phys.* **9**, 795–800 (2013).

40. C. S. Hamilton, R. Kruse, L. Sansoni, C. Silberhorn, I. Jex, Driven quantum walks. *Phys. Rev. Lett.* **113**, 083602 (2014).

41. E. Knill, R. Laflamme, G. J. Milburn, A scheme for efficient quantum computation with linear optics. *Nature* **409**, 46–52 (2001).

42. C. Vitelli, N. Spagnolo, L. Aparo, F. Sciarrino, E. Santamato, L. Marrucci, Joining the quantum state of two photons into one. *Nature Photon.* **7**, 521–526 (2013).

Science Advances

Quantum walks and wavepacket dynamics on a lattice with twisted photons

Filippo Cardano, Francesco Massa, Hammam Qassim, Ebrahim Karimi, Sergei Slussarenko, Domenico Paparo, Corrado de Lisio, Fabio Sciarrino, Enrico Santamato, Robert W. Boyd, and Lorenzo Marrucci

View the article online
https://www.science.org/doi/10.1126/sciadv.1500087
Permissions
https://www.science.org/help/reprints-and-permissions

Use of this article is subject to the Terms of service